Article

An Electromagnetic MEMS Energy Harvester Array with Multiple Vibration Modes

Huicong Liu [1], Tao Chen [1,*], Lining Sun [1] and Chengkuo Lee [2]

[1] Jiangsu Provincial Key Labratory of Advanced Robotics, and Collaborative Innovation Center of Suzhou Nano Science and Technology, Soochow University, Suzhou 215123, China; E-Mails: hcliu078@suda.edu.cn (H.L.); lnsun@suda.edu.cn (L.S.)

[2] Department of Electrical & Computer Engineering, National University of Singapore, 4 Engineering Drive 3, Singapore 117576, Singapore; E-Mail: elelc@nus.edu.sg

* Author to whom correspondence should be addressed; E-Mail: chent@suda.edu.cn; Tel.: +86-512-6758-7217.

Academic Editor: Cheng Luo

Abstract: This paper reports the design, micromachining and characterization of an array of electromagnetic energy harvesters (EHs) with multiple frequency peaks. The authors present the combination of three multi-modal spring-mass structures so as to realize at least nine resonant peaks within a single microelectromechanical systems (MEMS) chip. It is assembled with permanent magnet to show an electromagnetic-based energy harvesting capability. This is the first demonstration of multi-frequency MEMS EH existing with more than three resonant peaks within a limited frequency range of 189 to 662 Hz. It provides a more effective approach to harvest energy from the vibration sources of multiple frequency peaks.

Keywords: MEMS; energy harvester; electromagnetic; multi-frequency

1. Introduction

For wireless sensing nodes and electronic devices, one of the main concerns is the lifetime of the battery-powered system. With the fast development of microelectromechanical systems (MEMS) and low-power wireless sensor networks, vibration-based energy harvesters (EHs) are increasingly important as an alternative to batteries for long lasting time and environmental protection [1,2]. Previously, tremendous EHs based on piezoelectric, electromagnetic and electrostatic transduction principles have been

demonstrated with single dominant resonant frequency [3–10]. However, the practical vibration sources may exhibit multiple frequency peaks over a wide bandwidth [11]. The key issue is that the resonant frequency of the EH device mismatches ambient vibration frequencies. It is necessary to develop multi-frequency or wideband EHs to collect efficient energy from different vibration peaks [12–14].

The present multi-frequency approaches can be categorized into two major groups. A straightforward approach reported by Sari *et al.* [15] is to employ arrays of 35 oscillating cantilevers, and each has different resonant frequency. The electrical current will be generated by means of the relative movement between the coil coated on the cantilever and a fixed magnet. By adjusting the length increments so that they are sufficiently small, the EH device shows an overlapping multi-frequency spectrum from 4.2 to 5 kHz. Ferrari *et al.* [16] has reported a similar multi-frequency strategy by using three piezoelectric bimorphs. The resonant frequencies of the bimorphs are 113, 183 and 281 Hz, respectively. The results show the possibility of an overall broadened bandwidth of the EH array. The second approach is concentrated on multiple vibration modes, while each mode represents one resonant frequency. Ching *et al.* [17] and Liu *et al.* [18,19] have respectively employed spiral and circular spring structures connected with center mass to realize electromagnetic energy harvesting with three distinct vibration modes. Yang *et al.* [20] have attached multiple individual masses along a fixed-fixed beam for achieving multiple vibration modes of the device. Among these works, the multi-frequency MEMS devices were limited to be around three resonant peaks. Chew and Li [21] utilized nine off-the-shelf piezoelectric cantilevers and linked end-to-end to form a 3D spring structure. The experimental results showed at least seven resonant peaks from frequency range of 100 to 1000 Hz. However, the major problem is its large volume and the in-compatibility of MEMS technique.

In this paper, a subtle integration of harvesting array mechanism with multiple vibration modes is successfully implemented in a single MEMS chip. The chip is micromachined and assembled with permanent magnets to achieve electromagnetic induced energy harvesting capability. The EH device consisting of three distinct harvesters exhibits as many as nine resonant peaks. The design, micromachining and characterization of the EH device will be introduced and discussed subsequently in the following sections.

2. Design and Fabrication

2.1. Device Configuration

Figure 1a shows a 3D drawing of the proposed electromagnetic MEMS EH array. It consists of three distinct spring-mass structures, named as harvesters 1, 2, and 3. Each harvester contains a proof mass suspended by two folded springs located respectively at the up and down parts of the chip. The proof masses are patterned with spiral-shaped aluminum (Al) coils which are symmetrical about the center line. The double-layer Al coil of 10 μm in width and 1 μm in depth are isolated by Si_3N_4 layer on the Si chip. The up coil is connected to the corresponding up bonding pads through the up folded springs, while the down coil is similarly connected to their down bonding pads. Each folded spring contains 11 beams with the beam width of 30 μm, spacing of 70 μm, and thickness of 150 μm, while the width and thickness of each proof mass are 2.66 mm and 400 μm, respectively. The beam and mass lengths of the harvesters 1, 2 and 3 are 2.0, 2.9 and 2.1 mm, respectively, resulting in different resonance

ranges of these three harvesters. The overall MEMS EH chip size is 10 mm in length, 8 mm in width and 0.4 mm in thickness. In Figure 1b, the MEMS EH chip is bonded on a supporting base. Two cylindrical permanent magnets with diameter of 3 mm and height of 2 mm are placed on top of the harvester array via a supporting beam. When the three harvesters oscillate in different vibration modes, ambient vibration energy will be converted into electrical energy according to Faraday's law of induction.
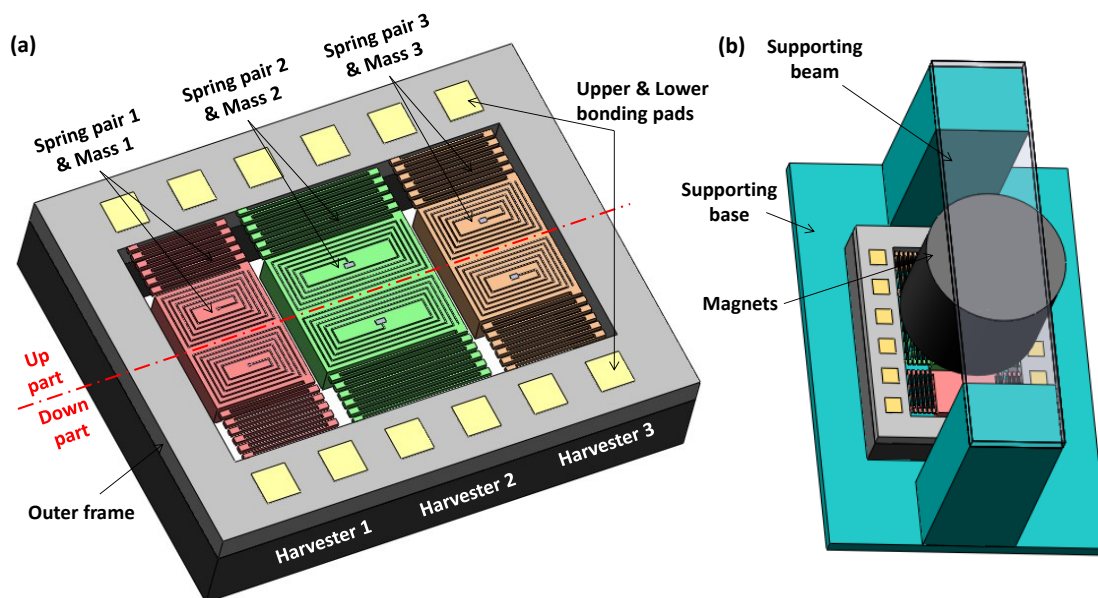

Figure 1. 3D drawing of (**a**) the proposed multi-frequency microelectromechanical systems (MEMS) energy harvester (EH) chip and (**b**) the assembled electromagnetic EH device.

2.2. Micromachining Process

Figure 2 shows the complementary metal oxide semiconductor (CMOS)-compatible micromachining process of the EH array. It starts from a silicon on insulator (SOI) wafer with a 150-µm-thick Si device layer, a 1-µm-thick buried oxide (BOX) layer and a 725-µm-thick Si handling layer. Firstly, the frontside surface of the SOI wafer is deposited with a 0.1-µm-thick Si_3N_4 insulation layer by plasma-enhanced chemical vapor deposition (PECVD) at 400 °C (Figure 2a). In Figure 2b, the bottom metal coils, bonding pads and metal via of 1-µm-thick Al are formed by physical vapor deposition (PVD) at 100 °C, patterning, and reactive ion etching (RIE) in succession. It should be noted that the Al coil has a relatively low melting temperature, *i.e.*, 660 °C, hence the follow-up processing temperature must be lower than 660 °C. Next, a 0.8-µm-thick Si_3N_4 layer, which serves as the electrical insulation, is deposited by PECVD. In Figure 2c, the top metal coils and bonding pads of 1-µm-thick Al are constructed by the similar processes as Figure 2b. Subsequently, a 0.8-µm-thick Si_3N_4 insulation layer is deposited by PECVD and pad openings are formed by RIE process. In Figure 2d, a 2-µm-thick SiO_2 layer is deposited by PECVD at 400 °C as a hard mask layer. Then the frontside features of spring pairs and masses are patterned by the RIE of the SiO_2, Si_3N_4 layers and the deep RIE of the 150-µm-thick Si device layer. Later on, the thickness of the SOI wafer is reduced to be around 400 µm by the backside grinding and polishing. In Figure 2e, a 2-µm-thick SiO_2 layer is deposited on the backside surface as the hard mask and the deep RIE steps are followed to pattern the Si handling layer. Finally, the remaining SiO_2 layers are dry etched by CHF_3 plasma as shown in Figure 2f, such that the spring-mass structures are completely released.
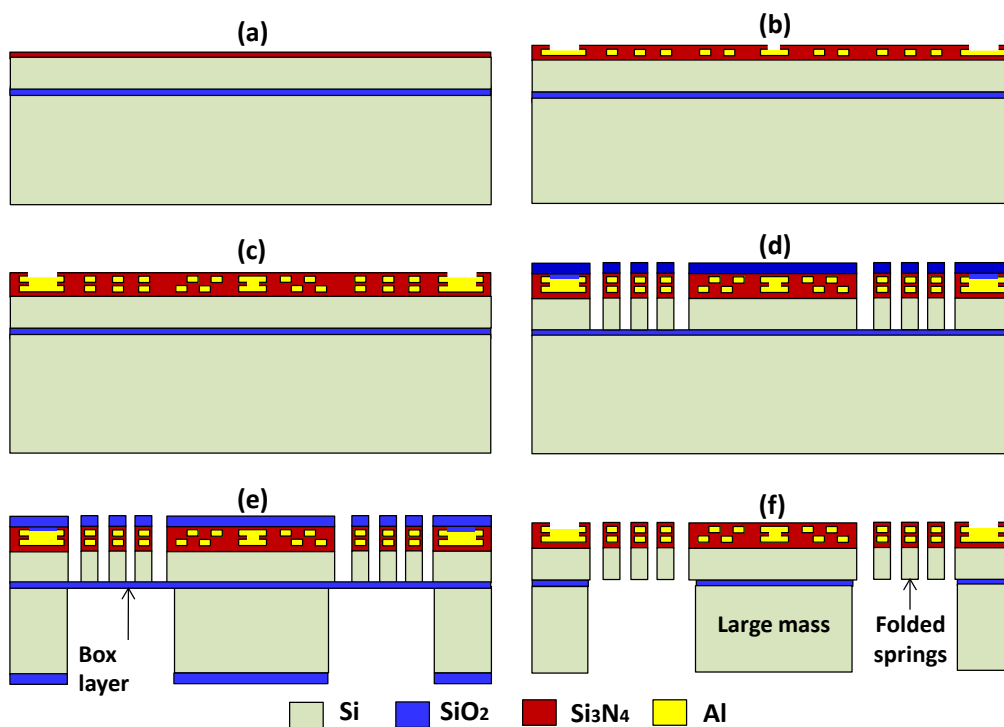
Figure 2. Microfabrication process of the EH array device. (**a**) Si_3N_4 deposition; (**b**) patterning of the 1st metal and isolation layers; (**c**) patterning of the 2nd metal and isolation layers; (**d**) frontside deep reactive ion etching (DRIE); (**e**) grounding and backside DRIE; (**f**) etch of SiO_2.

2.3. Mode Analysis

The mode analysis is conducted by finite element analysis software Abaqus. The first three vibration modes of each single harvester are found to be in-plane along *x*-axis at mode I, in-plane along *y*-axis at mode II and out-of-plane along *z*-axis at mode III. The EH array contains three harvesters with distinct dimensions of springs and masses. The larger spring length and mass of harvester 2 result in low resonant modes of 158 (at mode I), 346 (at mode II) and 377 (at mode III) Hz, respectively. By contrast, smaller spring-mass structures lead to relatively higher resonant modes, which are 368 (at mode I), 530 (at mode II) and 614 (at mode III) Hz respectively for harvester 1, and 295 (at mode I), 475 (at mode II) and 543 Hz (at mode III) respectively for harvester 3. Therefore, the overall vibration modes of the device are the combination of nine different resonances ranging from 158 to 614 Hz as listed in Table 1.

Table 1. Simulated vibration modes summary of the energy harvester (EH) array device.

EH Array	Mode I (In-plane)	Mode II (In-plane)	Mode III (Out-of-plane)
Harvester 1	368 Hz	530 Hz	614 Hz
Harvester 2	158 Hz	346 Hz	377 Hz
Harvester 3	295 Hz	475 Hz	543 Hz

3. Experiments and Discussion

The experiments are conducted by using a vibration control system as shown in Figure 3. It contains an electromagnetic shaker and a power amplifier, which produce vibrations at different frequencies and accelerations. The shaker is driven by using control software which sends a signal through a controller. The EH array device is assembled on an L-shaped plate and then fixed to the shaker, such that the vertical excitation of the shaker is along the *x*-axis of the MEMS chip. An accelerometer attached on the L-shaped plate is used to measure the acceleration level and sent the feedback signal to the controller. In the test, frequency sweeps are conducted from 50 to 800 Hz at a constant acceleration and the output voltages of the device are collected via a vibration control channel which is then transferred to the computer software using an ethernet port.

The open-circuit rms voltages of the EH array against frequencies for up and down coils are characterized at acceleration of 1 g along *x*-axis. It is obvious from Figure 4 that the overall voltage spectrum of the EH array shows nine resonant peaks ranging from 189 to 662 Hz. Due to the larger spring length and mass, harvester 2 produces relatively larger output voltages of 0.050, 0.105 and 0.035 mV for up coil at points A_2, B_2 and C_2, and 0.099, 0.127 and 0.120 mV for down coil at points D_2, E_2 and F_2, at the lower resonant frequencies of 189, 348 and 406 Hz, respectively. For harvester 3, the three resonant modes are 280, 379 and 479 Hz. The corresponding voltages are 0.05, 0.039 and 0.085 mV for up coil (points A_3, B_3 and C_3) and 0.042, 0.037 and 0.066 mV for down coil (points D_3, E_3 and F_3). For harvester 1, since the spring length is shorter and the mass is smaller, the three resonant modes of 382, 563 and 662 Hz are higher but the output voltages are relatively lower, which are 0.032, 0.013 and 0.036 mV for up coil (points A_1, B_1 and C_1) and 0.02, 0.014 and 0.043 mV for down coil (points D_1, E_1 and F_1). The enlarged scanning electron microscope (SEM) image is shown in Figure 3b. It is found that the spring beam is uneven etched which results in the frequency shift of the device comparing to the simulation results.

The open circuit voltage V_{rms} can be considered as the generated voltage of the harvester. Hence, the output power P is expressed as:

$$P = \left[\frac{V_{rms}}{R_L + R_C}\right]^2 \times R_L \tag{1}$$

As long as the load resistance R_L is matched with the internal resistance of the coil R_C, the maximum output power $P_{\max}$ is obtained as:

$$P_{\max} = V_{rms}^2/4R_C \tag{2}$$

The resistance of up and down coils for harvester 1, 2 and 3 are measured and the maximum output power and power density is calculated according to Equation (2). It is seen from Table 2 that the output voltage and power of current prototype is relatively low. Because the mass movement is relatively small for each harvester at different modes, the magnetic flux change across the limited coils is not significant. In addition, the winding coil is limited due to a very small mass area.
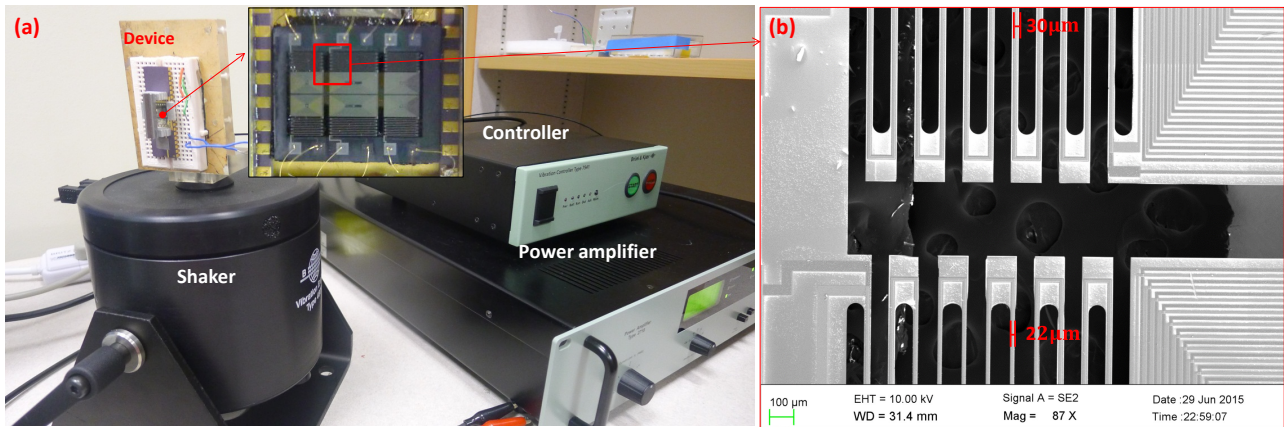
Figure 3. (**a**) A closed-loop vibration control system with assembled EH array device; (**b**) the scanning electron microscope (SEM) image of the enlarge spring.
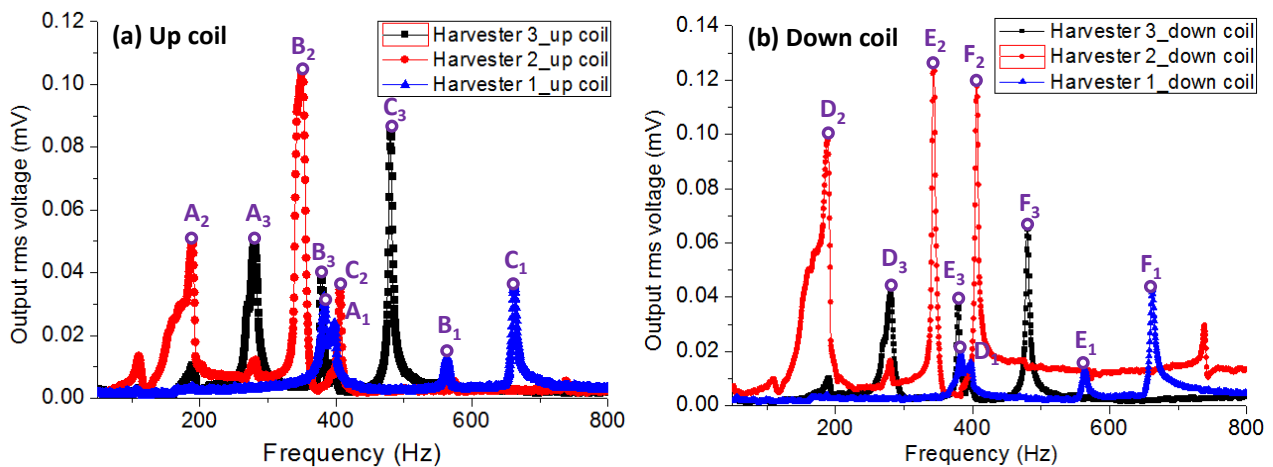

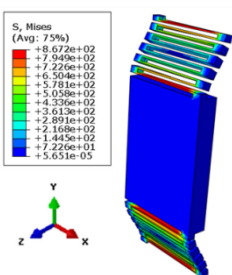**Figure 4.** The output voltages of the EH array against frequencies for (**a**) up and (**b**) down coils at acceleration of 1 *g* along *x*-axis.
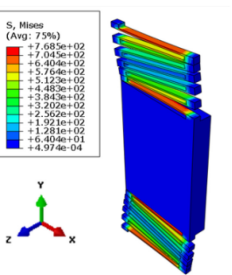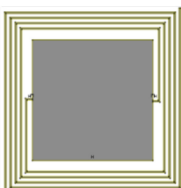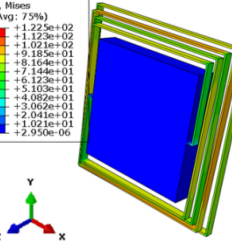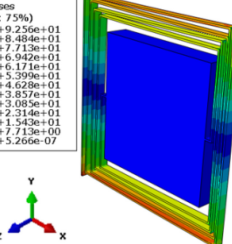
Table 2. Output performance summary of the EH array device.

EH Array	Resonant Modes (Hz)		Output rms Voltage (mV)		Power (μW)	Power Density (μW/cm³)
			Up Coil	Down Coil		
Harvester 1	Mode I	382	0.032	0.020	1.086×10^{-6}	0.034×10^{-3}
$R1_{up} = 362\ \Omega$	Mode II	563	0.013	0.014	0.303×10^{-6}	0.010×10^{-3}
$R1_{down} = 264\ \Omega$	Mode III	662	0.036	0.043	2.646×10^{-6}	0.083×10^{-3}
Harvester 2	Mode I	189	0.050	0.099	7.433×10^{-6}	0.232×10^{-3}
$R2_{up} = 457\ \Omega$	Mode II	348	0.105	0.127	16.012×10^{-6}	0.500×10^{-3}
$R2_{down} = 404\ \Omega$	Mode III	406	0.035	0.120	9.581×10^{-6}	0.299×10^{-3}
Harvester 3	Mode I	280	0.050	0.042	2.851×10^{-6}	0.089×10^{-3}
$R3_{up} = 428\ \Omega$	Mode II	379	0.039	0.037	1.968×10^{-6}	0.062×10^{-3}
$R3_{down} = 317\ \Omega$	Mode III	479	0.085	0.066	7.655×10^{-6}	0.239×10^{-3}

On the basis of current design concept of multi-mode harvesting array, future works will be conducted to further improve the output voltage and power, by optimizing the dimension of the spring-mass structures, the construction of the coil patterns and the distribution of the magnetic flux.

Firstly, the chip size and harvester array arrangement will be re-defined. The spring-mass structure will be optimized from folded springs to spiral springs [17] as shown in Table 3. Finite element analysis shows that the spiral springs have lower spring constant and lower stress concentration; thus, a larger displacement can be obtained and better fatigue loading can be endured. By the same means, not only can the coil area be increased, but also can the spring deformation or the mass displacement. Meanwhile, the spring stiffness as well as the resonant frequency is easy to be reduced or adjusted. Secondly, the patterned coil width and spacing can be further reduced from 10 to 5 μm. The increased coil density would greatly enhance the voltage output. Thirdly, the magnet will be changed from a circular bulk to a square array with alternating south and north poles and strong magnetic flux. The magnet array will be designed to match with the moving mass. In addition, the gap distance between the magnet and coil will be further reduced. In case of design optimization, a rough estimation of the obtained power can be several hundred times higher than the current prototype. Anyway, this prototype shows a promising design concept for multi-frequency MEMS energy harvester. However, high power generation of the device is still a great challenge and requires further exploration.

Table 3. Stress analysis for folded and spiral spring structures.

Total Frame Area 12.5 mm² Total Mass Area 5.3 mm²	Stress Distribution for Mass Displacement of $z = 1$ mm	Stress Distribution for Mass Displacement of $x = 0.5$ mm
Frame 2.5mm*5mm Mass 2mm*2.66mm	Maximum stress 867.2 MPa	Maximum stress 768.5 MPa
Frame 3.5mm*3.5mm Mass 2.3mm*2.3mm	Maximum stress 122.5 MPa	Maximum stress 92.56 MPa

4. Conclusions

A design of a multiple resonant frequency microstructure array for electromagnetic energy harvesting applications has been proposed. The EH array has been microfabricated and fully characterized using a closed-loop vibration control system. It is found that every microharvester has three resonant modes. By combining the three microharvesters with different dimensions, the EH array has at least nine noticeable resonant peaks from 100 to 800 Hz. The open-circuit output voltages at the three resonances are varying from 0.01 to 0.13 mV. This is the first demonstration of multi-frequency MEMS EH with nine resonant peaks. With further optimization in the design and dimensional

parameters, it is expected that the design would improve the effectiveness in harvesting the ambient kinetic energy from vibrations with multiple peaks.

Acknowledgments

Author Contributions

Huicong Liu, Tao Chen, and Lining Sun conceived and designed the experiments; Huicong Liu and Chengkuo Lee fabricated and provided the energy harvesting device; Huicong Liu performed the experiments, analyzed the data and images and wrote the paper.

Conflicts of Interest

The authors declare no conflict of interest.

References

1. Mitcheson, P.D.; Yeatman, E.M.; Rao, G.K.; Holmes, A.H.; Green, T.C. Energy Harvesting From Human and Machine Motion for Wireless Electronic Devices. *Proc. IEEE* **2008**, *96*, 1457–1486.
2. Matiko, J.W.; Grabham, N.J.; Beeby, S.P.; Tudor, M.J. Review of the application of energy harvesting in buildings. *Meas. Sci. Technol.* **2014**, *25*, 012002.
3. Aktakka, E.E.; Peterson, R.L.; Najafi, K. A CMOS-compatible piezoelectric vibration energy scavenger based on the integration of bulk PZT films on silicon. In Proceedings of 2010 IEEE International Electron Devices Meeting (IEDM), San Francisco, CA, USA, 6–8 December 2010.
4. Elfrink, R.; Kamel, T.M.; Goedbloed, M.; Matova, S.; Hohlfeld, D.; van Andel, Y.; van Schaijk, R. Vibration energy harvesting with aluminum nitride-based piezoelectric devices. *J. Micromech. Microeng.* **2009**, *19*, 094005.
5. Tang, G.; Liu, J.Q.; Yang, B.; Luo, J.B.; Liu, H.S.; Li, Y.G.; Yang, C.S.; He, D.N.; Dao, V.D.; Tanaka, K. Fabrication and analysis of high-performance piezoelectric MEMS generators. *J. Micromech. Microeng.* **2012**, *22*, 065017.
6. Kulkarni, S.; Koukharenko, E.; Torah, R.; Tudor, J.; Beeby, S.; O'Donnell, T.; Roy, S. Design, fabrication and test of integrated micro-scale vibration-based electromagnetic generator. *Sens. Actuators A Phys.* **2008**, *145*, 336–342.
7. Liu, H.C.; Gudla, S.; Hassani, F.A.; Heng, C.H.; Lian, Y.; Lee, C.K. Investigation of the Nonlinear Electromagnetic Energy Harvesters From Hand Shaking. *IEEE Sens. J.* **2015**, *15*, 2356–2364.
8. Feng, Y.; Hagiwara, K.; Iguchi, Y.; Suzuki, Y. Trench-filled cellular parylene electret for piezoelectric transducer. *Appl. Phys. Lett.* **2012**, *100*, 262901.

9. Suzuki, Y.; Miki, D.; Edamoto, M.; Honzumi, M. A MEMS electret generator with electrostatic levitation for vibration-driven energy-harvesting applications. *J. Micromech. Microeng.* **2010**, *20*, 104002.

10. Han, M.; Qiu, G.; Liu, W.; Meng, B.; Zhang, X.S.; Zhang, H. Note: A cubic electromagnetic harvester that convert vibration energy from all directions. *Rev. Sci. Instrum.* **2014**, *85*, 076109.

11. Roundy, S.; Wright, P.K.; Rabaey, J. A study of low level vibrations as a power source for wireless sensor nodes. *Comput. Commun.* **2003**, *26*, 1131–1144.

12. Han, M.; Li, Z.; Sun, X.; Zhang, H. Analysis of an in-plane electromagnetic energy harvester with integrated magnet array. *Sens. Actuators A Phys.* **2014**, *219*, 38–46.

13. Han, M.D.; Yuan, Q.; Sun, X.M.; Zhang, H.X. Design and Fabrication of Integrated Magnetic MEMS Energy Harvester for Low Frequency Applications. *J. Microelectromech. Syst.* **2014**, *23*, 204–212.

14. Nguyen, S.D.; Halvorsen, E.; Paprotny, I. Bistable springs for wideband microelectromechanical energy harvesters. *Appl. Phys. Lett.* **2013**, *102*, 023904.

15. Sari, I.; Balkan, T.; Kulah, H. An electromagnetic micro power generator for wideband environmental vibrations. *Sens. Actuators A Phys.* **2008**, *145*, 405–413.

16. Ferrari, M.; Ferrari, V.; Guizzetti, M.; Marioli, D.; Taroni, A. Piezoelectric multifrequency energy converter for power harvesting in autonomous microsystems. *Sens. Actuators A Phys.* **2008**, *142*, 329–335.

17. Ching, N.H.; Wong, H.Y.; Li, W.J.; Leong, H.W.; Wen, Z.Y. A laser-micromachined multi-modal resonanting power transducer for wireless sensing systems. *Sens. Actuators A Phys.* **2002**, *97–98*, 685–690.

18. Liu, H.; Soon, B.W.; Wang, N.; Tay, C.J.; Quan, C.; Lee, C. Feasibility study of a 3D vibration-driven electromagnetic MEMS energy harvester with multiple vibration modes. *J. Micromech. Microeng.* **2012**, *22*, 125020.

19. Liu, H.C.; Qian, Y.; Lee, C.K. A multi-frequency vibration-based MEMS electromagnetic energy harvesting device. *Sens. Actuators A Phys.* **2013**, *204*, 37–43.

20. Yang, B.; Lee, C.; Xiang, W.; Xie, J.; He, J.H.; Kotlanka, R.K.; Low, S.P.; Feng, H. Electromagnetic energy harvesting from vibrations of multiple frequencies. *J. Micromech. Microeng.* **2009**, *19*, 035001.

21. Chew, Z.; Li, L. Design and characterisation of a piezoelectric scavenging device with multiple resonant frequencies. *Sens. Actuators A Phys.* **2010**, *162*, 82–92.